



Research article

An essential update on the inventory of landslides triggered by the Jiuzhaigou Mw6.5 earthquake in China on 8 August 2017, with their spatial distribution analyses

Jingjing Sun^{a,b}, Xiaoyi Shao^{b,c}, Liye Feng^{a,b}, Chong Xu^{b,c,*}, Yuandong Huang^{b,c}, Wentao Yang^a

^a School of Soil and Water Conservation, Beijing Forestry University, Beijing, 100083, China

^b National Institute of Natural Hazards, Ministry of Emergency Management of China, 100085, Beijing, China

^c Key Laboratory of Compound and Chained Natural Hazards Dynamics, Ministry of Emergency Management of China, Beijing, 100085, China

ARTICLE INFO

Keywords:

Jiuzhaigou earthquake
Landslide catalogue
Spatial distribution
Coseismic landslide
Google Earth

ABSTRACT

On August 8, 2017, a magnitude Mw6.5 (Ms7.0) earthquake occurred in Jiuzhaigou County, Aba Prefecture, in the northern part of Sichuan Province, China, with a focal depth of 20 km and an epicenter located at (33.2°N, 103.8°E). Due to the significant magnitude of the earthquake, a large number of coseismic landslides were triggered. Despite previous research conducted by experts on the landslides caused by the Jiuzhaigou earthquake, the actual number of landslides has been severely underestimated in the previously published papers. Through field surveys and visual interpretation of high-resolution remote sensing images before and after the mainshock, we have established a detailed inventory of earthquake-induced landslides. The results indicate that the event caused a minimum of 9428 landslides covering a total area of 18.82 km². These landslides are mainly distributed in the IX intensity area of the earthquake. The landslides mainly consist of medium-sized landslides and debris flows. They predominantly occur in areas with an altitude ranging from 2600 m to 3600 m, with slopes greater than 30° and facing east and southeast. The Lower Carboniferous and Middle Carboniferous formations are more prone to triggering landslides, and landslides are more concentrated within 1 km of roads and in forested areas. Additionally, as the distance from roads and the epicenter increases, the values of LAP and LND decrease, indicating a positive correlation between the two. There are more landslides within 2 km from the fault and within a range of 6 km–9 km from the epicenter. In conclusion, this study provides a comprehensive landslide inventory with broader coverage and increased accuracy. It also conducts a comprehensive analysis of the spatial distribution patterns of landslides. This contributes to a deeper understanding of the causes of coseismic landslides and further research on the impact of landslides in affected areas.

1. Introduction

Earthquake-induced landslides are geological disasters caused by seismic activity, characterized by the occurrence of numerous large-scale landslide events and resulting in severe damage [1]. For instance: In 2014, the Mw6.2 earthquake in Ludian, Yunnan

* Corresponding author. National Institute of Natural Hazards, Ministry of Emergency Management of China, 100085, Beijing, China.
E-mail address: xc1111111@126.com (C. Xu).

<https://doi.org/10.1016/j.heliyon.2024.e24787>

Received 20 July 2023; Received in revised form 13 January 2024; Accepted 15 January 2024

Available online 20 January 2024

2405-8440/© 2024 The Authors. Published by Elsevier Ltd. This is an open access article under the CC BY-NC-ND license (<http://creativecommons.org/licenses/by-nc-nd/4.0/>).

triggered at least 10,559 coseismic landslides [2]. In 2016, the Mw7.8 earthquake occurred in the central part of the South Island of New Zealand, causing about 14,000 coseismic landslides [3]. In 2022, Ms5.8, Ms6.0 and Ms5.2 earthquakes will occur successively in Maerkang City, Aba Prefecture, Sichuan Province, China, triggering at least 650 coseismic landslides [4]. Due to the frequent occurrence of earthquakes, more and more researchers have begun to pay attention to this field [5]. With the continuous advancement and wide application of remote sensing and geographic information technology, the accumulation of landslide databases has gradually increased [6]. In this context, an accurate, objective, comprehensive, and scientifically compiled inventory map of earthquake-induced landslides plays a fundamental role in landslide-related research. Conducting extensive research on earthquake-induced landslides is crucial for enhancing our ability to mitigate hazards caused by earthquakes, safeguarding human lives and property, and preserving the ecological environment.

On August 8, 2017, a magnitude Mw6.5 (Ms7.0) earthquake occurred in Jiuzhaigou County, Aba Prefecture, northern Sichuan Province, China, with a focal depth of 20 km and an epicenter located at (33.2°N, 103.8°E). Due to its significant magnitude, the earthquake triggered a large number of coseismic landslides. After the earthquake, researchers have already conducted investigations on the numerous landslides triggered by the Jiuzhaigou earthquake. For example, at the beginning of the earthquake, Fan [7] et al. interpreted 1883 coseismic landslides based on a large number of high-resolution satellite images before and after the earthquake. Later, Wu [8] supplemented the coseismic landslides caused by the earthquake, ultimately identifying 2212 coseismic landslides. In 2019, Tian [9] further improved the accuracy and completeness of the interpretation and compiled a landslide inventory containing 4834 coseismic landslides. This inventory provided important scientific support for subsequent studies. However, due to the frequent rainy weather after the earthquake, it was difficult to obtain clear remote sensing images at that time. As a result, only about 4800 landslides were identified in previous studies. Although the successful identification of these landslides laid the foundation for subsequent papers on spatial distribution and susceptibility evaluation, it did not reflect the real situation enough. In view of this, this study is based on the 4834 landslides in Tian [9], and it is perfected. Based on the ultra-high resolution remote sensing images covering the entire earthquake area before and after the earthquake, and using the method of manual visual interpretation, a detailed landslide inventory map of the area was produced. Finally, we have compiled a thorough and all-encompassing catalog of landslides triggered by the Jiuzhaigou earthquake in Sichuan. We then proceeded to statistically analyze the factors influencing these landslides and characterize the distribution patterns of seismic landslides. The results of this study can support subsequent analysis of landslide susceptibility and provide a more accurate understanding of the relationship between seismic activity and landslide occurrence.

2. Study area overview

Since the Late Cenozoic, the Indian Plate has been moving towards the Eurasian Plate at a continuous speed, resulting in collision and compression of the Eurasian Plate. This has led to the formation of the complex geological structure of the Qinghai-Tibet Plateau [9]. Fig. 1 (a) shows the distribution of seismic activities with magnitudes above Ms5.0 within the Qinghai-Tibet Plateau. It includes the 2010 Ms7.1 earthquake in Yushu, the 2008 Ms8.0 earthquake in Wenchuan, the 2013 Ms7.0 earthquake in Lushan, the 2014 Ms6.5 earthquake in Ludian, and others. In this active seismic tectonic background, the occurrence of the Jiuzhaigou earthquake was driven, making in-depth research on this earthquake crucial for enhancing our understanding of strong seismic activity in the Qinghai-Tibet Plateau region.

Jiuzhaigou is situated in the northwest of Sichuan Province. The Jiuzhaigou earthquake occurred in the northern segment of the North-South seismic zone, which is located between the Qinghai-Tibet Plateau and the Sichuan Basin, forming a deeply incised high mountain gorge zone. This region is part of one of China's most active tectonic units and is a key seismic zone [11,12]. From a regional tectonic perspective, due to the obstruction from the South China block, the Bayan Har block has experienced intense crustal deformation in this area. The eastern end of the East Kunlun fault exhibits a noticeable southward deflection and has formed a broom-shaped extension with multiple branch faults intersecting with the Longriba fault, Minjiang fault, and Huya fault [13]. Over time, the fault activity has gradually transitioned from strike-slip to thrust [14]. Along the boundaries of the blocks, several strong earthquakes have

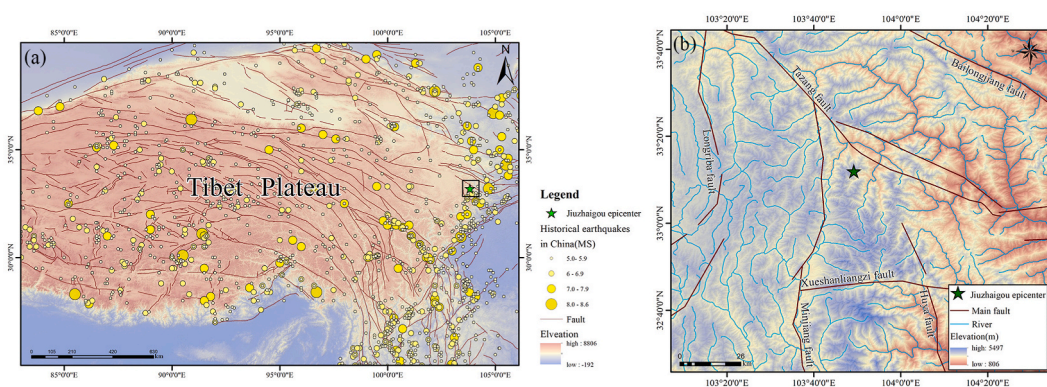


Fig. 1. Tectonic setting of the 2017 Jiuzhaigou Earthquake [10] (a) Historical earthquake points on the Qinghai-Tibet Plateau (data from China Earthquake Network), (b) Major fault zones within the epicenter.

occurred. Therefore, in this study area, the structures of active faults are highly complex due to the influence of intense shear stress [15]. As shown in Fig. 1(b), the epicenter is surrounded by two branch faults of the East Kunlun fault zone, the Tazang fault (NW trending), the Minjiang fault (NS trending), and the Xueshanliangzi fault (EW trending) [16,17]. Based on the analysis of the regional seismic tectonic environment and combined with the emergency investigation data of the Jiuzhaigou earthquake, the causative fault is identified as a nearly 330° -trending, southwest-dipping, upright left-lateral strike-slip fault [18,19]. It is one of the main controlling factors for crustal movement and seismic activity in the region. The valleys in Jiuzhaigou County are widely distributed, with higher elevations in the northwest and southwest parts, and relatively lower elevations in the southeast.

3. 3. data and method

3.1. Remote sensing interpretation

Visual interpretation and AI-based automatic extraction are commonly used methods for landslide interpretation. The automatic landslide extraction is fast and short, with a high degree of automation and adjustable parameters [6]. However, its disadvantage is that it is technically complex and factors such as remote sensing image type, regional geomorphological features and landslide type will affect its accuracy. Therefore, this method is more suitable for emergency response activities in the immediate aftermath of an earthquake, and is not suitable for areas with complex geomorphology that are highly affected by earthquakes. In many current studies, visual interpretation is still widely applied [1,20,21]. Although visual interpretation is time-consuming, it can provide a more objective and accurate interpretation of the affected area, and has a better ability to objectively recognize targets in areas with complex geomorphology. In this study, we fully utilized human resources and time to visually interpret the research area, resulting in a rich and accurate database.

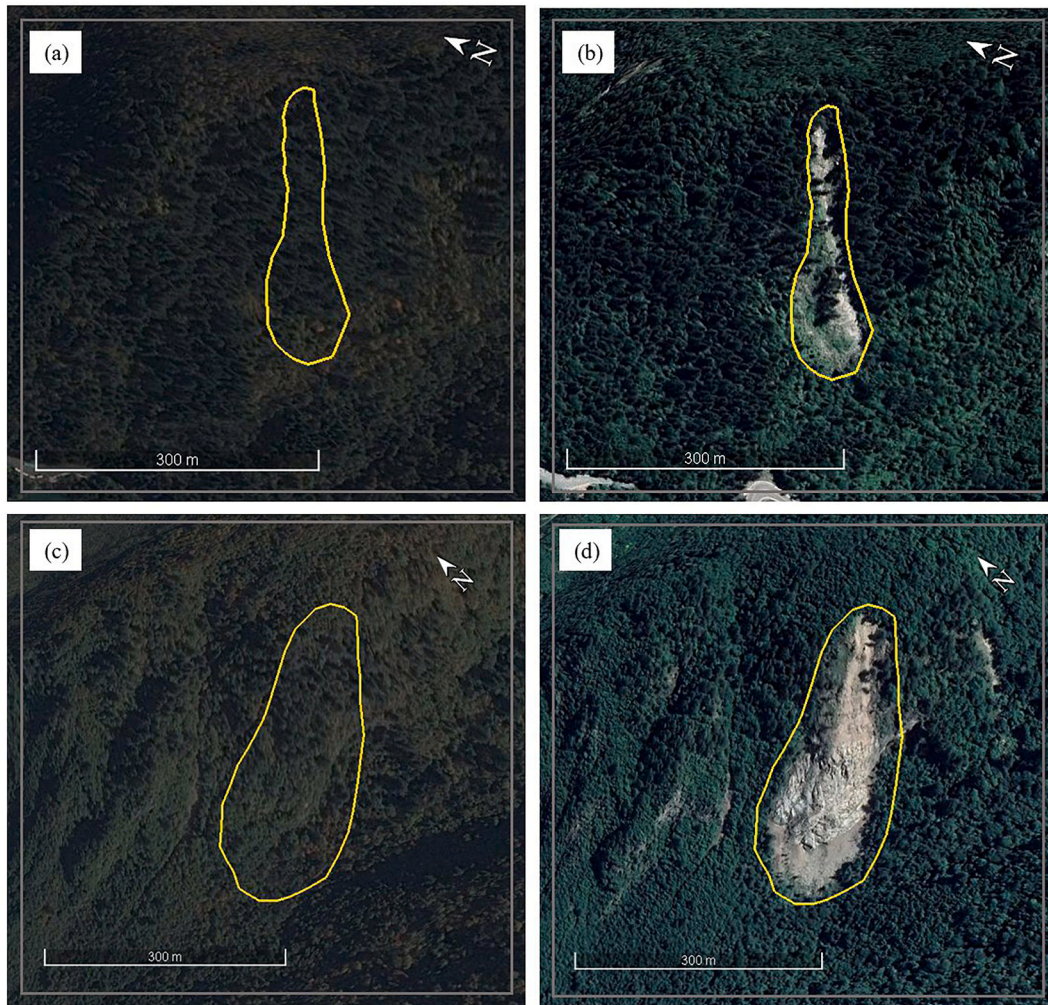


Fig. 2. Comparison of images before and after a typical landslide earthquake. (a)–(b) $103^\circ53'1''E$ $33^\circ9'33''N$ (c)–(d) $103^\circ56'32''E, 33^\circ16'38''N$.

After the 2017 Jiuzhaigou earthquake, to date, some high-resolution low-cloud and ultra-high-resolution low-cloud aerial photographs and satellite images have become available resources. For example, the Google Earth platform can provide high-resolution stereo satellite images at different times after the earthquake, covering the entire study area and publicly accessible. Based on this, in this study, we utilized the Google Earth platform and conducted visual interpretation and comparison of pre- and post-earthquake images in the study area. As shown in Fig. 2(a) and (c) are pre-earthquake images, and Fig. 2(b) and (d) are post-earthquake images. It can be observed that there is high vegetation cover in the pre-earthquake image and low or no vegetation cover in the post-earthquake image, and there are clear signs of sliding, identifying the area as an earthquake-induced landslide and delineating it as a polygonal area.

3.2. Environmental factors

Terrain, geology, and seismic activity are important factors that induce coseismic landslides. Based on the characteristics and research objectives of the Jiuzhaigou region, we selected terrain factors, including elevation, slope, aspect, and position. The DEM data used were sourced from "ALOS PALSAR 12.5 m DEM". Slope and aspect factors were extracted from the DEM data using GIS platforms. Position refers to the geomorphic features that describe relative location and specific slope surface shapes. To classify slope positions, we adopted the rules proposed by Weiss [22], which divide them into six categories: ridge, upper slope, middle slope, lower slope, valley slope, and valley. Geologic factors include lithology, distance from road and land use. In the study area, roads are mostly constructed along the alignment, and their excavation may decrease slope stability. Therefore, the distance from roads was also considered. The lithology of the study area is based on the 1:200,000 geological map, and the accuracy of the land use data is 30 m. Seismic factors include distance from the epicenter, distance from the seismogenic fault, and seismic intensity. The study area's seismic intensity zones are classified as zones VII, VIII, and IX, covering a total area of 4298 km². The China Seismological Network Center (www.ceic.ac.cn) provided the earthquake intensity and earthquake center required for this study. The thematic map of the seismogenic fault was created by constructing a buffer zone with a buffer distance of 2 km. Utilizing visually interpreted landslide polygon data, we extracted attribute values such as quantity and area. GIS was used to analyze environmental factors and provide corresponding values for the landslide locations. These values were later used in the subsequent statistical analysis.

4. Results and analysis

4.1. Landslide inventory

Combined with visual interpretation of remote sensing images from the Google Earth platform, the overall distribution of landslides is shown in Fig. 3. A total of 9428 landslides were identified, with their distribution mainly concentrated in intensity zones VII, VIII, and IX, covering an area of 4,298 km², and a total landslide area of 18.82 km². Landslides in intensity zone VII are scattered, while they are primarily concentrated in zones VIII and IX. Most of these mountainous landslides occurred in the eastern and southeastern regions of the epicenter, with another concentrated area in the northwest. In contrast, landslides are less concentrated in the northeast and southwest regions. Fig. 3(b) shows an enlarged image of the selected area, indicating a more concentrated distribution of landslides. The largest landslide has an area of 237,408 m², while the smallest measures 6.53 m², as shown in Fig. 4(a). There are 79 landslides with areas exceeding 20,000 m², accounting for 0.84% of the total. Additionally, there were 248 landslides, accounting for 2.63% of the total, with a combined area exceeding 11,000 square meters. The majority of landslides have areas less than 3000 m², representing 83.31% of the total. Fig. 4(b) provides a detailed breakdown of landslides with areas less than 3000 m². Among them, there are 5295

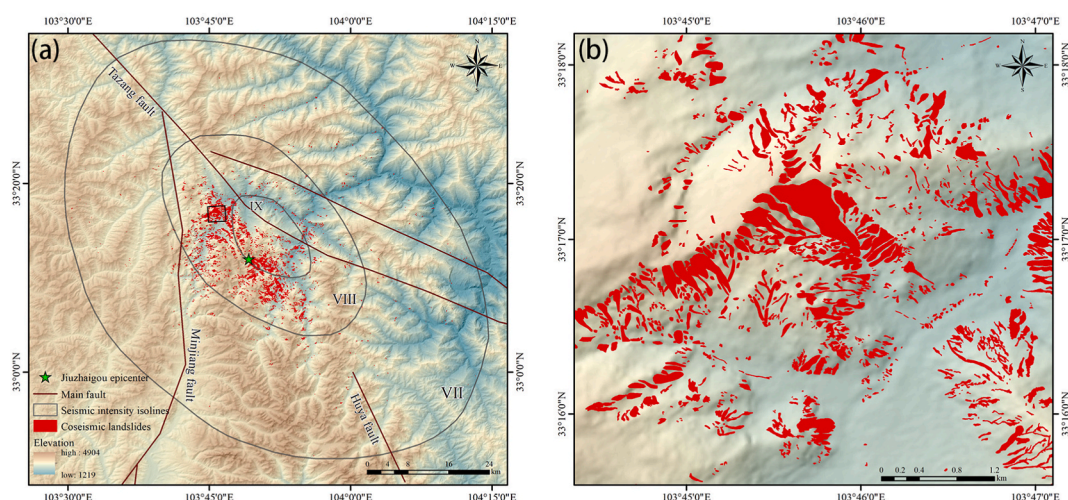


Fig. 3. (a) Landslide distribution map (b) Enlarged view of the black framed area in (a).

landslides with areas less than 1000 m², accounting for 67.42%. The highest proportion falls within the range of 200 m²–400 m², representing 18.04%.

Landslide volume is typically estimated using the area-volume relationship proposed in statistical studies [23]. We used the area-volume formula to estimate the volume of this landslide, and the estimated result was that the total volume of the landslide was 150 million cubic meters. Based on the total number of landslides, their areas, and volumes, the density of landslides in the study area was calculated to be 2.19 km⁻², with an area density of 0.44% and a volume density of 0.035 m. Fig. 5 illustrates the frequency-area curve of coseismic landslides on a logarithmic scale under ideal conditions. It can be expressed as:

$$\text{Lg } N = a \times \text{Lg } A + b \tag{1}$$

Among them, N represents the number of landslides, A represents the landslide area, and a and b are constants. Fig. 5 demonstrates the good completeness of the Jiuzhaigou earthquake landslide database. The fitting relationship of all values on the logarithmic coordinate axis is consistent with the ideal state, with a high regression coefficient (R²) of 0.821, indicating a relatively complete corresponding landslide inventory. The R² value for landslides with an area less than 3000 m² is 0.869, while for landslides with an area greater than 3000 m², the R² value is as high as 0.95. The proximity of the R² value to 1 reflects the goodness of fit and represents the completeness of the landslide inventory. According to the picture, the R² value for landslides larger than 3000 m² is close to 1, indicating that even in a relatively complete coseismic landslide database, some small-sized and low-mass landslides have not been identified.

4.2. Spatial distribution

LND (landslide number density) and LAP (landslide area percentage) are indicators used to measure the concentration and relative size of landslides under different control factors. By dividing the influencing factors into different parts, we can observe that they may show differences, and then analyze the data content. The proportion of landslide area can more intuitively reflect the distribution of landslides in each interval. Therefore, we selected LND, LAP and the proportion of landslides as the three indicators to evaluate the spatial distribution characteristics of Jiuzhaigou earthquake landslides to evaluate the distribution of landslides.

$$\text{LND} = \frac{\text{Landslide number}}{\text{The classification area of the factor interval(CA)}} \tag{2}$$

$$\text{LAP} = \frac{\text{Landslide area}}{\text{The classification area of the factor interval(CA)}} \tag{3}$$

4.2.1. Topographic factors

In this study, we used elevation, slope, aspect, and position as topographic factors. As depicted in Fig. 6(a), the elevation in the study area ranged from 1318 m to 4842 m. The elevation was divided into 13 intervals, excluding two intervals below 2000 m and above 4200 m. The remaining 11 intervals were spaced 200 m apart. The statistical results, presented in Fig. 6(b), demonstrate that both LND and LAP initially increase and then decrease with elevation. LND reaches its peak value of 4.85 km⁻² in the elevation range of 2800 m–3000 m, while LAP reaches its peak value of 0.90% in the range of 3000 m–3200 m. These two intervals cover a total area of 736.78 km², with a total of 3354 landslides occurring and a landslide area of 6.49 km², accounting for 17.36% and 18.21% of the total number of landslides, respectively. The highest concentration of landslides is observed between 2600 m and 3600 m, spanning an area of 14.31 km², which accounts for 77.67% of the total landslide area.

As shown in Fig. 7(a), the slope range in the study area is from 0° to 82.79°, with the maximum slope angle of 78.89° observed within the study area. Each 10° interval is divided into a slope interval. As shown in Fig. 7(b) and (d), LND has an obvious positive

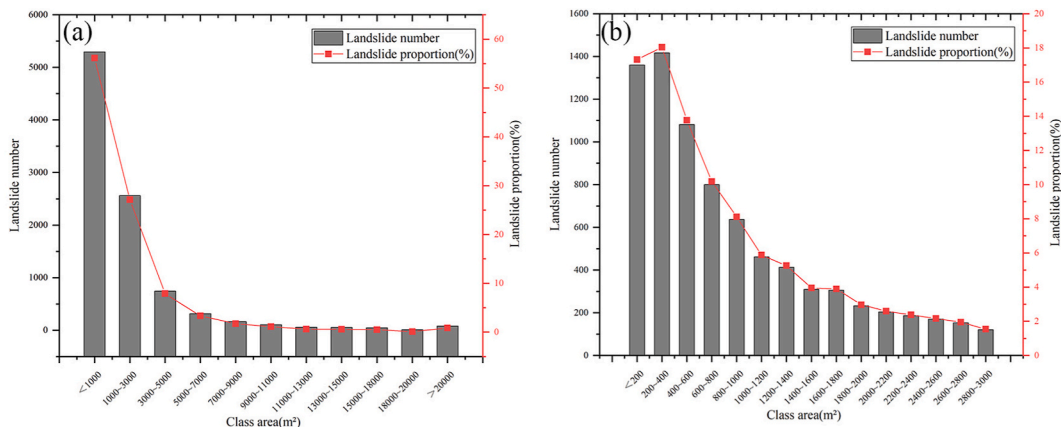


Fig. 4. Number and proportion of landslides. (a) All landslides. (b) Landslides with an area of less than 3000 m².

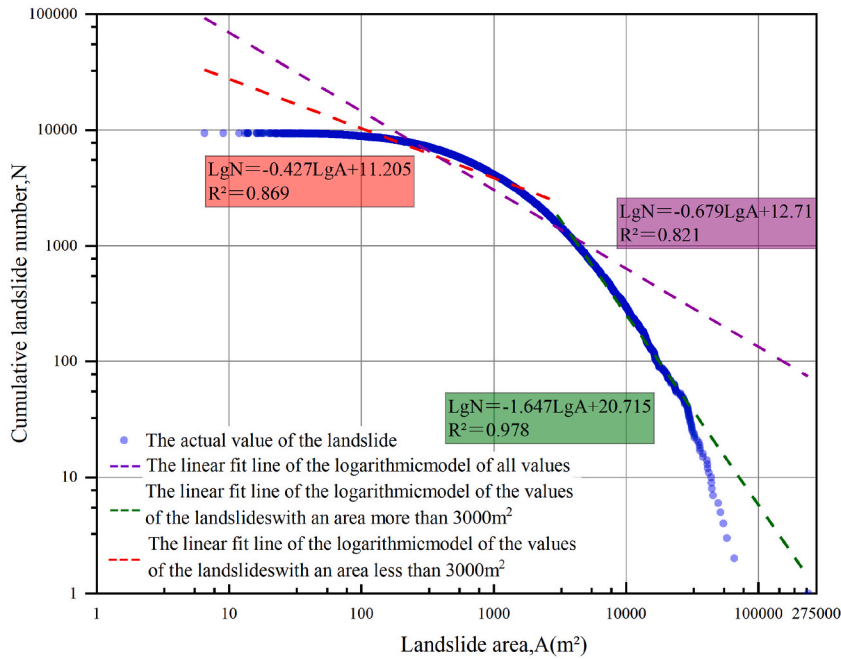


Fig. 5. Correlation between the cumulative landslide number and the landslide area related to the Jiuzhaigou earthquake.

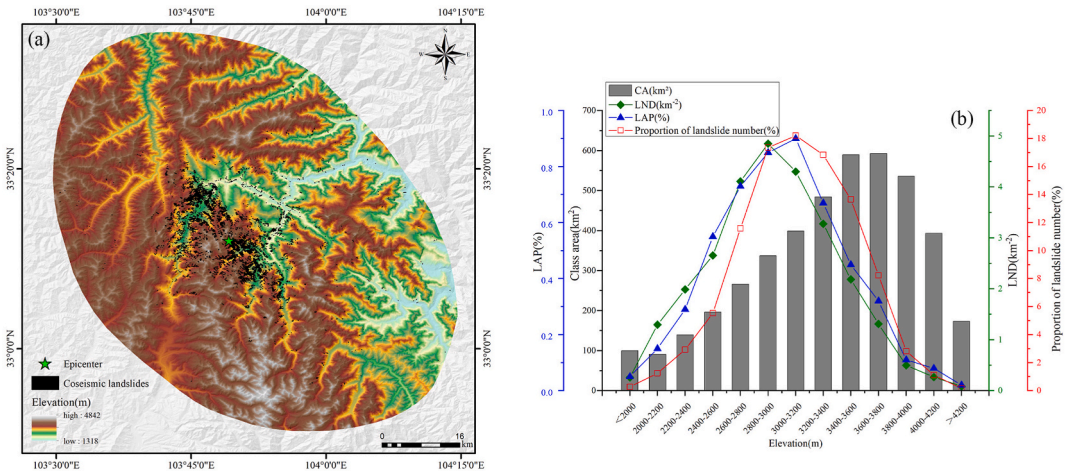


Fig. 6. Analysis of influencing factors: elevation. (a) Elevation and landslide locations. (b) Statistical analysis results.

correlation with slope, and within the range of 70°–80°, LND reaches a maximum value of 11.15 km⁻². LAP is also positively correlated with slope within a specific range, reaching its peak in the 60°–70° range. Additionally, Fig. 7(c) and (e) show the landslide area reaches its maximum value in the range of 40°–50°, as this interval has the highest number of landslides, accounting for 35.22% of the total. 66.79% of the landslides were concentrated in the 30°–50° range. It is observed that as the slope angle increases, the number and area of landslides decrease, which is consistent with the typical characteristics of earthquake-induced landslides.

As shown in Fig. 8(a), slope positions are divided into 6 categories, but landslides have not been distributed on Gentle Slopes, so we only conducted the analysis on the other 5 categories. As shown in Fig. 8(b), LND reaches its peak on the Upper Slopes at 2.39 km⁻², indicating a higher likelihood of landslide occurrence on this slope position. LAP is most prevalent on Steep Slopes, at 0.48%. The majority of landslides are concentrated on the Steep Slopes, accounting for a high percentage of 63.95% on this slope position.

As shown in Fig. 9(a), the north direction is set as 0°, and the slope direction is divided into nine categories. The slope angle is associated with specific directions. Fig. 9(d) and (e) demonstrate that LND and LAP reach their highest values in the southeast direction, at 3.29 km⁻² and 0.72%, respectively. This is due to the presence of numerous large-scale landslides within this range. Fig. 9 (b) and (c) show the landslides are concentrated in the east and southeast directions, covering an area of 7.6 km², accounting for 38.25% of the total landslides.

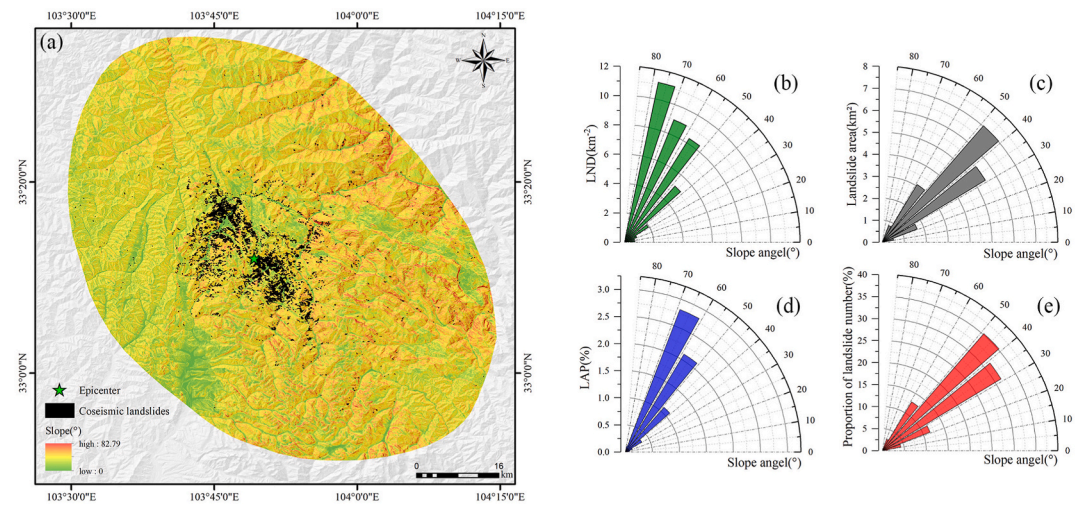


Fig. 7. Analysis of influencing factors: slope angel. (a) Slope angel and landslide locations. (b)–(e) Statistical analysis results.

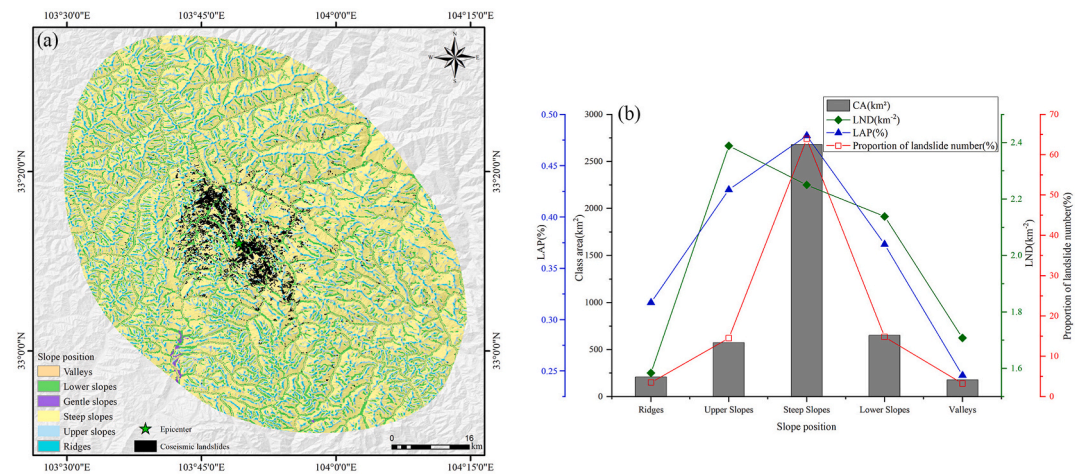


Fig. 8. Analysis of influencing factors: slope position. (a) Slope position and landslide locations. (b) Statistical analysis results.

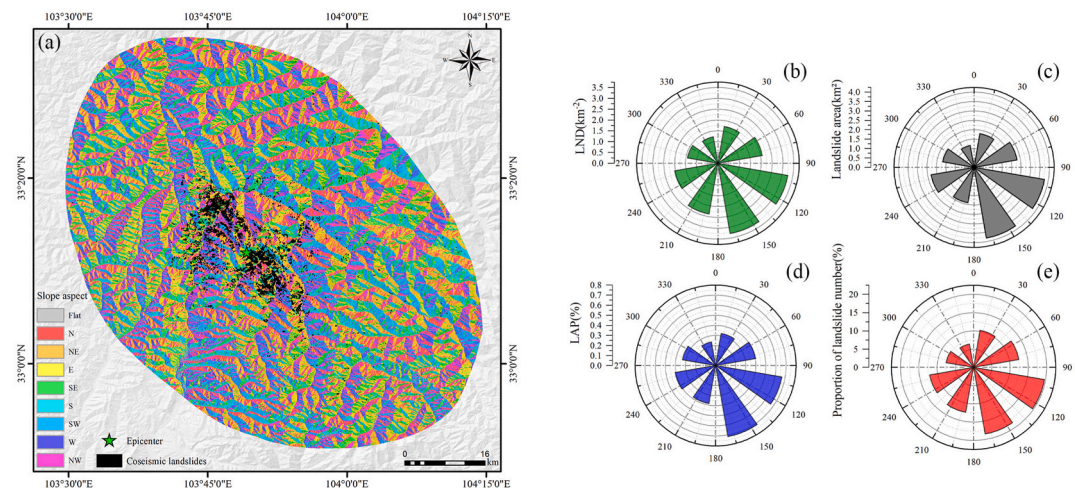


Fig. 9. Analysis of influencing factors: slope aspect. (a) Slope aspect and landslide locations. (b)–(e) Statistical analysis results.

4.2.2. Geological factor

Based on previous research, we selected three geological factors, namely lithology, distance from roads, and land use, for analysis. Lithology influences slope stability and strength and plays a crucial role in the occurrence and distribution of co-seismic landslides. Due to the complexity of lithology, we divided it into nine intervals based on stratigraphic age, as shown in Table 1 and Fig. 10(a). The statistical analysis is presented in Fig. 10(b). The results indicate significant differences in landslide development among different geological formations. The Middle Triassic (T2) triggered a total of 621 landslides, covering an area of 1546.17 km², which is the highest among all formations. The Middle Carboniferous (C2) experienced the most landslides, with 2565 occurrences and a total area of 137.38 km², with LND and LAP accounting for 18.67 km⁻² and 3.98%, respectively, which is much higher compared to other stratigraphic ages. It can be observed that the T2 triggered a large number of large landslides, while the Lower Carboniferous (C1) had the highest number of triggered landslides, accounting for 37.75% of the total, but with relatively smaller average areas. The variation in landslide density and area among different geological formations indicates that lithology plays a crucial controlling role in the development of co-seismic landslides.

Fig. 11(a) and (b) demonstrates that the closer the distance to roads, the more co-seismic landslides occur. Within a 1 km range from the highway, LND and LAP reach their maximum values, indicating that engineering activities during road construction may alter the terrain and slope stability. The farther away from roads, the fewer co-seismic landslides occur, and both the landslide count and the LND and LAP show a decreasing trend. This suggests that roads play an important role in the distribution of co-seismic landslides.

As shown in Fig. 12(a) and (b), Grassland exhibits the highest LAP value of 0.56%, indicating that Grassland is more susceptible to landslides compared to other land types. On the other hand, Shrubland shows the highest LND value of 2.90 km⁻², suggesting more frequent landslide activities in this region. Forest areas have a higher number of landslides, accounting for 60.73% of the total, mainly because of the larger overall area covered by forests. Additionally, the higher LND and LAP values in the Forest region indicate that it is the primary affected area of the Jiuzhaigou earthquake.

4.2.3. Earthquake factor

Earthquake intensity provides a visual representation of the impact of earthquakes on the geological environment in a particular region. In this study, as shown in Fig. 13(a), landslides were located within the regions of intensity VII, VIII, and IX, as shown in Fig. 13 (b), which presents the distribution of landslide counts, LND, and LAP indices for different intensity zones. From the graph, it is evident that landslides are most concentrated in intensity zone VIII, covering an area of 764.03 km², with a total of 6346 landslide occurrences and an area of 13.04 km², accounting for 67.31% of the total landslides. As for LAP and LND, intensity zone IX has the highest proportion, accounting for 3.03% and 15.94%, respectively.

Seismic wave energy is a direct factor contributing to co-seismic landslides, while the fault ruptures during earthquakes are the focus of earthquake disaster research and play a crucial role in energy transfer. In this paper, the distance from the fault rupture was divided into intervals of 2 km each, as shown in Fig. 14(a). According to the results of Fig. 14(b), as the distance from the fault rupture increases, the landslide indicators show an overall decreasing trend. Among them, the interval within 0–2 km from the fault rupture has the highest number of landslides, with 4602 occurrences, covering an area of 9.38 km², and accounting for 48.81% of the total landslides. The highest values for LAP and LND both appear within the 0–2 km range, at 4.12% and 20.21 km⁻², respectively.

The third seismic factor considered is the distance from the epicenter, and Fig. 15(a) divides this distance into intervals of 3 km each to establish buffer zones, resulting in 12 intervals. The result is shown in Fig. 15(b), LAP gradually decreases with an increase in distance from the epicenter, reaching its peak value within the 3 km range from the epicenter at 6.87%. LND, on the other hand, shows an overall decreasing trend but exhibits a slight increase within the from 3 km to 6 km and 6 km–9 km ranges. Landslides are most numerous within the 6 km–9 km ranges, with 2924 occurrences, accounting for 31.01% of the total landslides.

5. Discussion

5.1. Jiuzhaigou landslide database

Previous research has provided interpretations of landslides in the Jiuzhaigou area. Table 2 presents the available landslide

Table 1
Lithological classification.

Lithology No.	Category	Main Lithology
C1	Lower Carboniferous	Layered limestone, Shale, Slate
C2	Middle Carboniferous	Phyllite, Limestone
C3	Upper Carboniferous	Shale, Limestone, Clay rock
T1	Lower Triassic	Limestone, Slate
T2	Middle Triassic	Limestone, Slate, Dolomite
T3	Upper Triassic	Sandstone, Slate
D	Devonian	Limestone, Quartz sandstone, Sandy slate
N	Neogene	Conglomerate, Siltstone, Sandstone
P	Permian	Layered limestone, Dolomites, Phyllite
Q	Quaternary	Dolomite, Siltstone, Pebble
γ	Pre-Jurassic	Granite, Amphibole

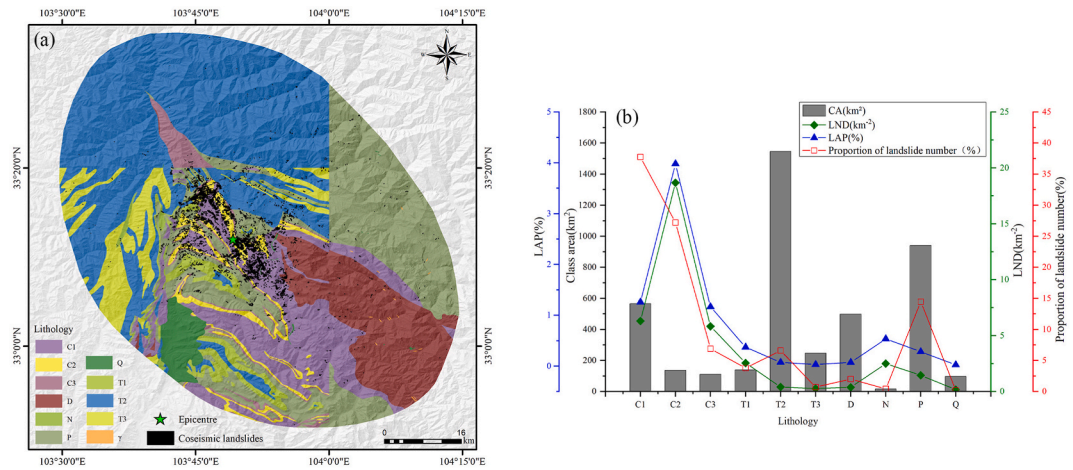


Fig. 10. Analysis of influencing factors: lithology. (a) Lithology and landslide locations. (b) Statistical analysis results.

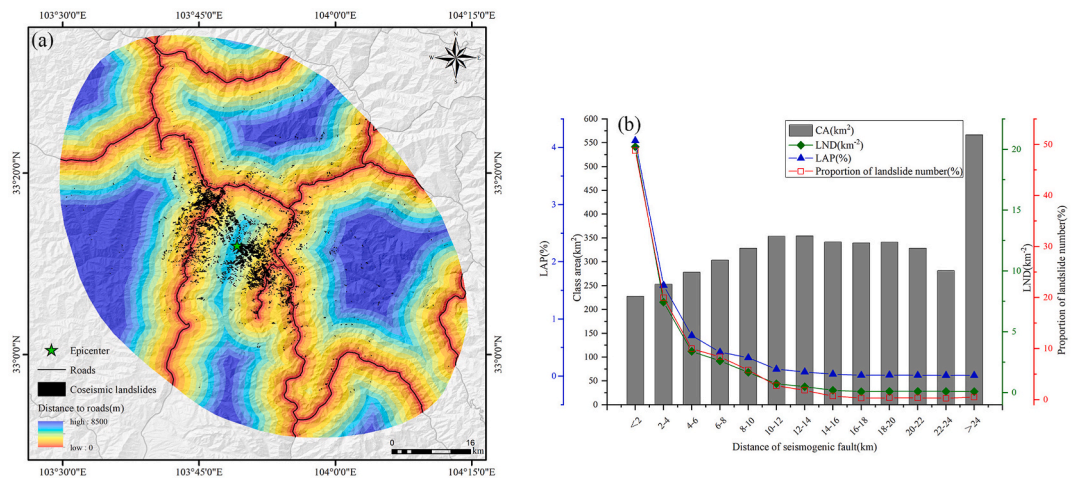


Fig. 11. Analysis of influencing factors: distance from the roads. (a) The distance from the roads and landslide locations. (b) Statistical analysis results.

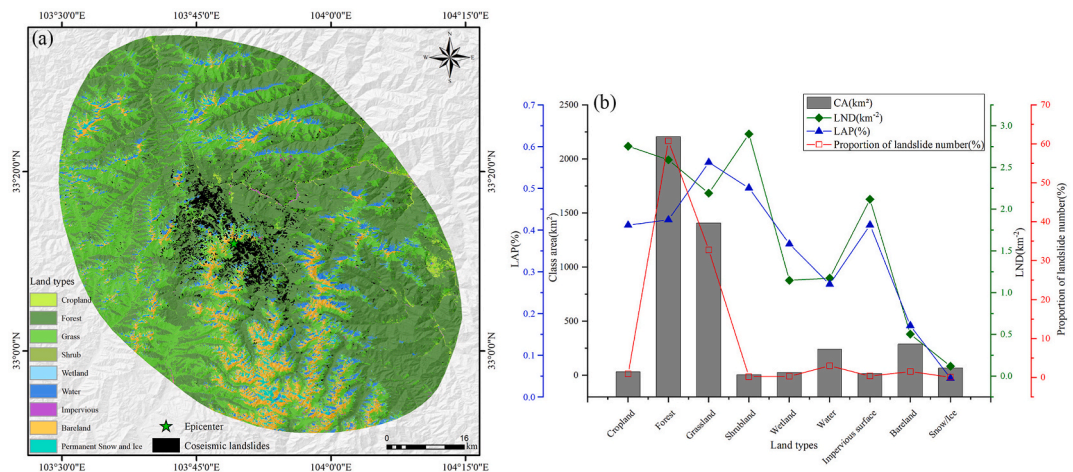


Fig. 12. Analysis of influencing factors: land use type. (a) Land use type and landslide locations. (b) Statistical analysis results.

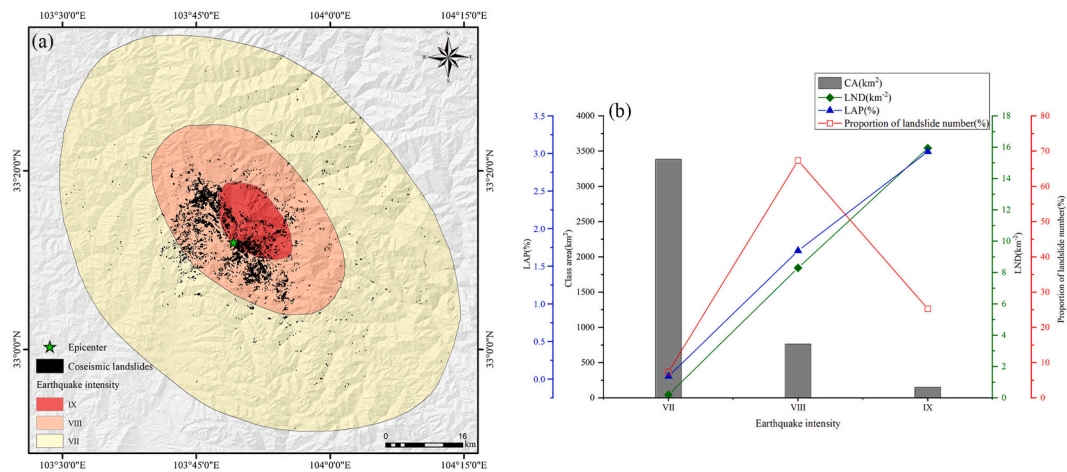


Fig. 13. Analysis of influencing factors: earthquake intensity. (a) Earthquake intensity and landslide locations. (b) Statistical analysis results.

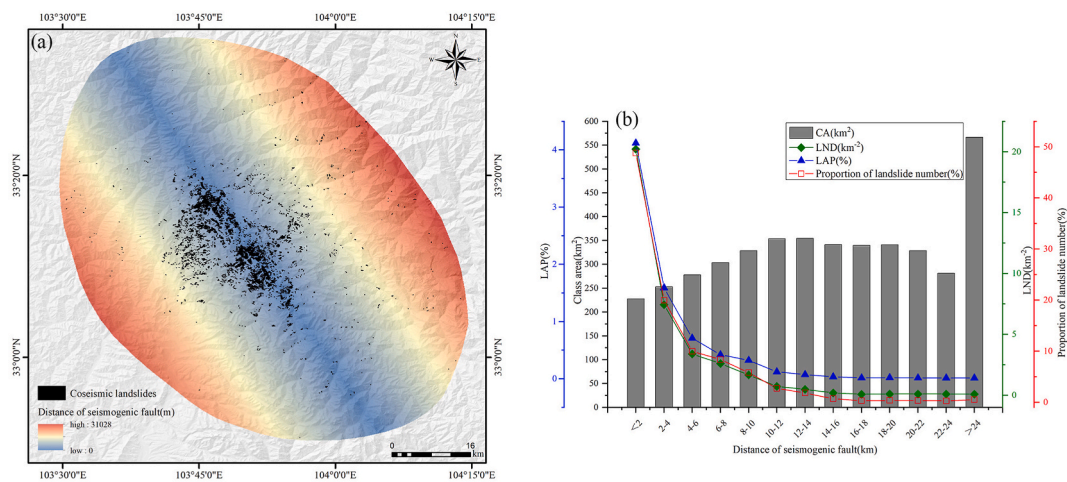


Fig. 14. Analysis of influencing factors: distance from the seismogenic fault. (a) The distance from the seismogenic fault and landslide locations. (b) Statistical analysis results.

database results covering the entire seismic area that can be retrieved. This table displays various investigation findings related to the Jiuzhaigou earthquake-induced landslides, including different sources, distribution areas, landslide counts, total landslide areas, and the maximum/minimum landslide areas within the study area. First, we can observe that there are differences in the selection of study areas among different studies. For example, Zhang [24] chose a more extensive distribution area, covering 5288 km². While Tian [9] focused on a smaller study area, which was only 434 km². This indicates that different studies may have different emphases and considerations for the investigation scope of earthquake landslides. In addition, there is significant variation in the number of landslides reported in different studies. This table indicates that our study documented the highest number of landslides, with a total of 9,428, while the lowest recorded number of landslides was only 681 [25]. The reasons for such discrepancies in landslide counts are threefold. Firstly, some studies may have smaller study areas, resulting in fewer interpreted landslides. Secondly, there may be differences in visual interpretation criteria for identifying landslides. Thirdly, the interpretation of landslides may depend on different landslide images used in different articles. For instance, Dai [26] utilized aerial images of varying resolutions and high-resolution images (Geoeye-1, 0.5 m) as the basis for their study, but their coverage was relatively small, primarily concentrated on the north-east side of the epicenter. Tian [9] relied on high-resolution Geoeye-1 images (0.5 m) for landslide interpretation. Li [27] used Sentinel-2A imagery for co-seismic landslide identification and assisted the interpretation with high-resolution Google imagery (Geoeye-1, 0.3 m). The provision of high-quality imagery before and after earthquakes has enhanced the capability to identify and observe landslides triggered by seismic activities in the region.

This study builds upon the work of Tian [9] to further interpret landslides. To showcase the research results, we selected a specific area (Fig. 16) to compare the landslide interpretations. Fig. 16(a) shows the landslides interpreted by Tian, while Fig. 16(b) presents the landslide interpretations based on this study's criteria. By comparing the red boxed areas in Fig. 16(a) and (b), it is evident that

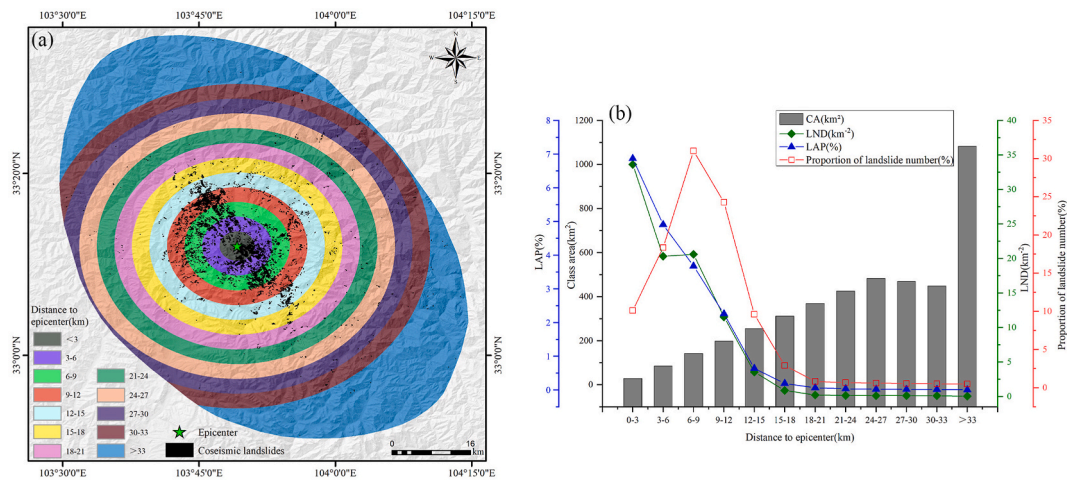


Fig. 15. Analysis of influencing factors: distance from the epicenter. (a) The distance from the epicenter and landslide locations. (b) Statistical analysis results.

Table 2
Evaluate previous research on landslides induced by the 2017 Jiuzhaigou Earthquake.

No.	Distribution area (km ²)	Landslide number	Total area (km ²)	Max. area (m ²)	Min. area (m ²)	Sources
1	840	1883	8.11	231,000	9.7	[26]
2	1275	2212	11.80	231297.3	9.7	[8]
3	–	1780	–	–	–	[12]
4	651.3	2212	11.80	209,000	10	[28]
5	434	4834	9.64	236338.3	7.8	[9]
6	546.85	681	–	200,000	80	[25]
7	5288	6205	16.67	260,000	13.6	[24]
8	1840	5633	14.10	239,000	15	[29]
9	541.61	821	3.92	–	–	[30]
10	2055	4456	13.7	–	–	[31]
11	653	1022	3.88	64,700	10.21	[32]
12	938.9	5431	9.45	243,000	6.0	[15]
13	1330	5487	10.56	243,000	5.5	[27]
This study	4298	9428	18.82	237,408	6.5	–

Tian only interpreted one landslide in the boxed area, whereas this study identified eleven landslides. The landslide interpretations in this study surpass Tian’s findings in terms of accuracy and objectivity. The landslide catalog in this study covers an area of 4298 square kilometers. Compared with previous studies, the distribution area is wider, indicating that this study examines more geographical ranges and improves the comprehensiveness of the study. Secondly, this study recorded 9428 landslides. Compared with previous studies, the number of landslides has increased significantly. This is due to the fact that the post-earthquake imagery used in this paper is a multi-phase fusion of planet (resolution: 3 m) imagery, which is dated within three months after the earthquake, and is also corrected in conjunction with Google Earth imagery. By using high-resolution remote sensing imagery with minimal cloud cover,

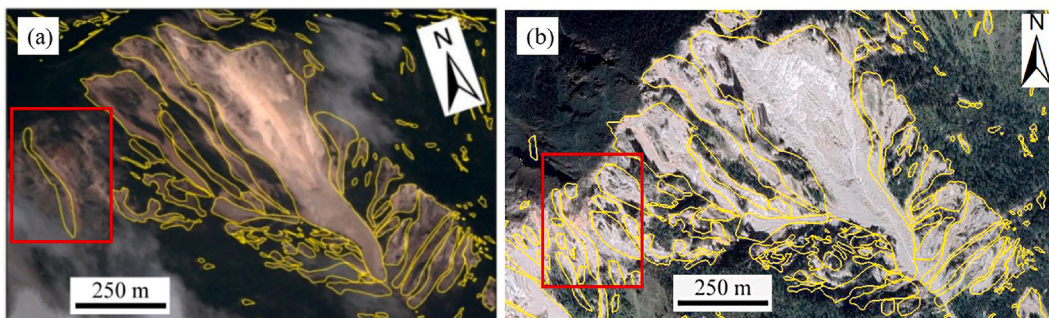


Fig. 16. Comparison chart of interpretation results of landslide triggered by Jiuzhaigou earthquake. (a) The landslides interpreted by Tian [9]. (b) The landslides interpreted by this study.

clearer and more detailed geomorphic features can be obtained, enabling more accurate capture and analysis of earthquake-induced landslide boundaries, morphology, and changes. This is the primary reason why this study has a higher landslide count than previous databases.

5.2. The significance of coseismic landslide database

According to the principles of landslide databases presented by Xu [33], accurate recording of landslide counts is crucial for obtaining an approximate estimation of landslide density and volume, aiding in a comprehensive understanding of co-seismic landslide phenomena. Incomplete landslide distribution data may mislead our understanding of landslide characteristics, susceptibility, hazard assessment, and further research. In light of the frequent earthquakes in recent years, accompanied by the release of significant energy, destructive co-seismic landslides have occurred one after another. Table 3 presents the major earthquake-induced landslide database achievements since the 2008 Wenchuan earthquake. A co-seismic landslide database, on one hand, provides information on landslide quantity, area, distribution, and the relationships with influencing factors. These data and analysis results contribute to understanding the scale, extent, and distribution patterns of landslide disasters. Through the study of landslide databases, spatial distribution characteristics and trends of co-seismic landslides can be revealed, helping to identify high-risk areas and zones susceptible to landslides. Additionally, the landslide database provides information about factors that trigger landslides, such as earthquake parameters, geological conditions, and topographic features, which play a significant role in the occurrence and evolution of landslides. On the other hand, as the most fundamental analytical data, the landslide database lays the foundation for subsequent studies on landslide susceptibility and hazards. For example, Havenith [34] et al. conducted in-depth investigations on the seismotectonic and climatic influences and conducted size-frequency relationship studies based on the Haiti landslide database [35]. Xu [36] and colleagues applied and validated a logistic regression model for landslide hazard assessment in Yushu earthquake based on the Yushu landslide database [37]. Wu [38] analyzed landslide susceptibility following the Ludian earthquake based on the Ludian landslide database [2]. Building upon the Jiuzhaigou landslide inventory by Tian [9] a series of follow-up studies were conducted, including Liu [39] conducted a comparative study involving convolutional neural networks and traditional machine learning methods for landslide susceptibility mapping. Ma [40] Study the hazard assessment of earthquake-induced landslide using a logistic regression model. Yang [41] and colleagues' conducts in-depth study of landslide susceptibility using a CNN-3D algorithm, and Chen [42] application of the Newmark model to evaluate earthquake-triggered landslides. These studies further explored various aspects of earthquake-induced landslides utilizing the landslide inventory data from previous researchers.

In summary, co-seismic landslide databases play a crucial role in landslide research, earthquake disaster assessment, and provide valuable data resources for scientific research and practical applications. As needs change, landslide inventory can not only provide a comprehensive assessment of the potential risk of seismic hazards, but can also be applied to multiple fields. For example, in urban planning, landslide inventory data can be used to better consider landslide risk and avoid large-scale construction in areas of potential landslide hazard. Landslide cataloging can also be utilized for monitoring the potential impacts of climate change on geohazards and to help develop adaptation strategies to address climate change. The results of this study have provided abundant data and important

Table 3
Database results of major earthquakes and landslides after 2008.

No.	Time	Earthquake location	Magnitude (Mw/Ms)	Landslide number	Total landslide area (km ²)	Sources
1	2008.05.12	Wenchuan, Sichuan, China	Mw7.9	197,481	1160	[43]
				56,000	811	[44]
2	2008.06.14	Iwate-Miyagi, Japan	Mw6.9	4161	–	[45]
3	2010.01.12	Port-au-Prince, Haiti	Mw7.0	30,828	15.736	[46]
				23,567	24.69	[35]
4	2010.04.14	Yushu, Qinghai, China	Mw7.9	2036	1.194	[37]
5	2011.09.18	Sikkim, India	Mw6.9	1196	–	[47]
6	2013.04.20	Lushan, Sichuan, China	Ms7.0	22,528	18.88	[48]
7	2013.07.22	Min County, Gansu, China	Ms6.6	6478	1.71	[49]
8	2014.04.15	Kumamoto, Japan	Mw7.0	3467	6.9	[50]
9	2014.08.03	Ludian, Yunnan, China	Ms6.5	12,817	16.33	[51]
10	2014.10.07	Jinggu, Yunnan, China	Ms6.6	441	1.08	[52]
11	2015.04.25	Kathmandu, Nepal	Ms8.1	47,200	110	[53]
				19,332	61.52	[54]
12	2017.08.08	Jiuzhaigou, Sichuan, China	Mw6.5	4834	9.64	[9]
				9428	18.82	本研究
13	2017.11.18	Miling, Tibet, China	Mw6.4	3130	19.76	[55]
14	2018.02.25	Papua New Guinea	Mw7.5	10,469	145	[56]
15	2018.09.06	Hokkaido, Japan	Mw6.6	12,586	41.1	[57]
				9295	30.96	[58]
16	2018.09.28	Papua, Indonesia	Mw7.5	15,700	43	[59]
17	2019.06.17	Changning, Sichuan, China	Ms6.0	496	1.2	[60]
18	2021.05.21	Yangbi, Yunnan, China	Mw6.4	95	0.1	[61]
19	2021.08.14	Nippes, Haiti	Mw7.2	8444	45.6	[62]
20	2022.06.10	Barkam, Sichuan, China	Ms6.0	650	1.2	[4]
21	2022.09.05	Luding, Sichuan, China	Ms6.8	5007	17.36	[63]

foundational information for the research on the Jiuzhaigou earthquake-induced landslides in Sichuan Province, China, offering scientific evidence for earthquake disaster prevention and emergency management, which carries significant meaning and value.

6. Conclusion

This study presents a comprehensive, objective, and accurate new database of the landslides triggered by the Jiuzhaigou earthquake on August 8, 2017. The database was created by manually interpreting high-resolution pre- and post-earthquake remote sensing images on the Google Earth platform, resulting in the identification of 9428 earthquake-induced landslides with a total area of 18.82 km². Among them, the largest individual landslide has an area of 237,408 m², and the smallest is 6.53 m², with the majority concentrated in the intensity zone IX.

Additionally, this research analyzes the distribution characteristics of co-seismic landslides from three aspects: topography, geology, and seismic factors. The results indicate that landslides occur within the elevation range of 2600 m–3600 m and on slopes with gradients between 30° and 50°, primarily facing east and southeast directions. Landslides are more likely to occur in steep slope areas. The Lower Carboniferous and Middle Carboniferous periods, areas within 1 km of roads, and forested regions show a higher density of landslides. Furthermore, landslides are more numerous in areas closer to the fault rupture, and the region 6 km–9 km from the epicenter exhibits significant landslide development. These findings hold crucial significance for further research on the Jiuzhaigou earthquake-induced landslides and their distribution characteristics.

Data availability statement

The coseismic landslide inventory in this paper is available from the corresponding author on reasonable request.

CRediT authorship contribution statement

Jingjing Sun: Writing – review & editing, Writing – original draft, Visualization, Validation, Software, Project administration, Methodology, Investigation, Formal analysis, Data curation, Conceptualization. **Xiaoyi Shao:** Data curation, Conceptualization. **Liye Feng:** Investigation, Formal analysis. **Chong Xu:** Supervision, Project administration, Funding acquisition, Formal analysis, Data curation, Conceptualization. **Yuandong Huang:** Software, Data curation. **Wentao Yang:** Supervision, Software.

Declaration of competing interest

The authors declare that they have no known competing financial interests or personal relationships that could have appeared to influence the work reported in this paper.

Acknowledgments

This study was supported by the National Natural Science Foundation of China (42077259) and the National Key Research and Development Program of China (2021YFB3901205).

References

- [1] Y. Huang, C. Xie, T. Li, C. Xu, X. He, X. Shao, X. Xu, T. Zhan, Z. Chen, An open-accessed inventory of landslides triggered by the Ms6.8 Luding earthquake, China on September 5, 2022, *Earthq. Res. Adv.* 3 (2023) 100181, <https://doi.org/10.1016/j.eqrea.2022.100181>.
- [2] W. Wu, C. Xu, X. Wang, Y. Tian, F. Deng, Landslides triggered by the 3 August 2014 Ludian (China) Mw6.2 earthquake: an updated inventory and analysis of their spatial distribution, *J. Earth Sci.* 31 (2020), <https://doi.org/10.1007/s12583-020-1297-7>.
- [3] H. Tanyas, T. Görüm, I. Fadel, C. Yıldırım, L. Lombardo, An open dataset for landslides triggered by the 2016 Mw7.8 Kaikōura earthquake, New Zealand, *Landslides* 19 (2022) 1405–1420, <https://doi.org/10.1007/s10346-022-01869-9>.
- [4] Z. Chen, Y. Huang, X. He, X. Shao, L. Li, C. Xu, S. Wang, X. Xu, Z. Xiao, Landslides triggered by the 10 June 2022 Maerkang earthquake Swarm, Sichuan, China: spatial distribution and tectonic significance, *Landslides* (2023) 1–15, <https://doi.org/10.1007/s10346-023-02080-0>.
- [5] X. Xu, C. Xu, Natural hazards research: an eternal subject of human survival and development, *Nat. Hazards Res.* 1 (2021) 1–3, <https://doi.org/10.1016/j.nhres.2020.12.003>.
- [6] C. Xu, T. Gorum, H. Tanyas, Application of remote sensing and GIS in earthquake-triggered landslides, *Front. Earth Sci.* 10 (2022) 964753, <https://doi.org/10.3389/feart.2022.964753>.
- [7] X. Fan, G. Scaringi, Q. Xu, W. Zhan, L. Dai, Y. Li, X. Pei, Q. Yang, R. Huang, Coseismic landslides triggered by the 8th August 2017 Ms7.0 Jiuzhaigou earthquake (Sichuan, China): factors controlling their spatial distribution and implications for the seismogenic blind fault identification, *Landslides* 15 (2018) 967–983, <https://doi.org/10.1007/s10346-018-0960-x>.
- [8] C. Wu, P. Cui, Y. Li, I.A. Ayala, C. Huang, S. Yi, Seismogenic fault and topography control on the spatial patterns of landslides triggered by the 2017 Jiuzhaigou earthquake, *J. Mt. Sci.* 15 (2018) 793–807, <https://doi.org/10.1007/s11629-017-4761-9>.
- [9] Y. Tian, C. Xu, S. Ma, X. Xu, S. Wang, H. Zhang, Inventory and spatial distribution of landslides triggered by the 8th August 2017 Mw6.5 Jiuzhaigou earthquake, China, *J. Earth Sci.* 30 (2019) 206–217, <https://doi.org/10.1007/s12583-018-0869-2>.
- [10] X. Xu, G. Chen, Q. Wang, L. Chen, Z. Ren, C. Xu, Z. Wei, R. Lu, X. Tan, S. Dong, Discussion on seismogenic structure of Jiuzhaigou earthquake and its implication for current strain state in the Southeastern Qinghai-Tibet Plateau, *Chin. J. Geophys.* 60 (2017) 4018–4026, <https://doi.org/10.6038/cjg20171028>.
- [11] J. Sun, H. Yue, Z. Shen, L. Fang, Y. Zhan, X. Sun, The 2017 Jiuzhaigou earthquake: a complicated event occurred in a young fault system, *Geophys. Res. Lett.* 45 (2018) 2230–2240, <https://doi.org/10.1002/2017GL076421>.
- [12] B. Zhao, Y. Wang, Y. Luo, J. Li, X. Zhang, T. Shen, Landslides and dam damage resulting from the Jiuzhaigou earthquake (8 August 2017), Sichuan, China, *R. Soc. Open Sci.* 5 (2018) 171418, <https://doi.org/10.1098/rsos.171418>.

- [13] S. Chen, J. Zhao, Q. Xu, H. Liu, C. Ju, Evidence for fluids at the hypocenter of the 2017 Ms7.0 Jiuzhaigou earthquake revealed by local earthquake tomography, *J. Geophys. Res. Solid Earth* 126 (2021) e2020JB021036, <https://doi.org/10.1029/2020JB021036>.
- [14] W. Peng, X. Huang, Z. Wang, Coseismic deformation and fault inversion of the 2017 Jiuzhaigou Ms7.0 earthquake: constraints from steerable pyramid and InSAR observations, *Rem. Sens.* 15 (2022) 222, <https://doi.org/10.3390/rs15010222>.
- [15] X. Wang, H. Mao, Spatio-temporal evolution of post-seismic landslides and debris flows: 2017 Ms7.0 Jiuzhaigou earthquake, *Environ. Sci. Pollut. Res.* (2022) 1–22, <https://doi.org/10.1007/s11356-021-16789-9>.
- [16] D. Li, Z. Ding, Y. Zhan, P. Wu, L. Chang, X. Sun, Upper crustal velocity and seismogenic environment of the M7.0 Jiuzhaigou earthquake region in Sichuan, China, *Earth Planet. Phys.* 5 (2021) 348–361, <https://doi.org/10.26464/epp2021038>.
- [17] F. Long, G. Yi, S. Wang, Y. Qi, M. Zhao, Geometry and tectonic deformation of the seismogenic structure for the 8 August 2017 Ms7.0 Jiuzhaigou earthquake sequence, Northern Sichuan, China, *Earth Planet. Phys.* 3 (2019) 253–267, <https://doi.org/10.26464/epp2019027>.
- [18] L. Fang, J. Wu, J. Su, M. Wang, C. Jiang, L. Fan, W. Wang, C. Wang, X. Tan, Relocation of Mainshock and aftershock sequence of the Ms7.0 Sichuan Jiuzhaigou earthquake, *Chin. Sci. Bull.* 63 (2018) 649–662, <https://doi.org/10.1360/N972017-01184>.
- [19] L. Han, J. Cheng, Y. An, L. Fang, C. Jiang, B. Chen, Z. Wu, J. Liu, X. Xu, R. Liu, Preliminary report on the 8 August 2017 Ms7.0 Jiuzhaigou, Sichuan, China, earthquake, *Seismol. Res. Lett.* 89 (2018) 557–569, <https://doi.org/10.1785/0220170158>.
- [20] L. Li, C. Xu, Z. Yang, Z. Zhang, M. Lv, An inventory of large-scale landslides in Baoji City, Shaanxi Province, China, *Data* 7 (2022) 114, <https://doi.org/10.3390/data7080114>.
- [21] X. Zhang, L. Li, C. Xu, Large-scale landslide inventory and their mobility in Lvliang City, Shanxi Province, China, *Nat. Hazards Res.* 2 (2022) 111–120, <https://doi.org/10.1016/j.nhres.2022.05.002>.
- [22] A. Weiss, Topographic position and landforms analysis, in: *Poster Presentation, ESRI User Conference, San Diego, CA, 2001*.
- [23] C. Xu, X. Xu, L. Shen, Q. Yao, X. Tan, W. Kang, S. Ma, X. Wu, J. Cai, M. Gao, Optimized volume models of earthquake-triggered landslides, *Sci. Rep.* 6 (2016) 29797, <https://doi.org/10.1038/srep29797>.
- [24] Q. Zhang, S. Ling, X. Li, C. Sun, J. Xu, T. Huang, Comparison of landslide susceptibility mapping rapid assessment models in Jiuzhaigou County, Sichuan province, China, *J. Rock Mech. Eng.* 39 (2020) 1595–1610, <https://doi.org/10.13722/j.cnki.jrme.2020.0029>.
- [25] Y. Yi, Z. Zhang, W. Zhang, Q. Xu, C. Deng, Q. Li, GIS-based earthquake-triggered-landslide susceptibility mapping with an integrated weighted index model in Jiuzhaigou Region of Sichuan Province, China, *Nat. Hazards Earth Syst. Sci.* 19 (2019) 1973–1988, <https://doi.org/10.5194/nhess-19-1973-2019>.
- [26] L. Dai, Q. Xu, X. Fan, M. Chang, Q. Yang, F. Yang, J. Ren, A preliminary study on spatial distribution patterns of landslides triggered by Jiuzhaigou earthquake in sichuan on august 8th, 2017 and their susceptibility assessment, *J. Eng. Geol.* 25 (2017) 1151–1164, <https://doi.org/10.13544/j.cnki.jeg.2017.04.030>.
- [27] Y. Li, L. Xu, L. Zhang, Z. Lu, N. Su, Study on development patterns and susceptibility evaluation of coseismic landslides within mountainous regions influenced by strong earthquakes, *Earth Sci.* 48 (2023) 1960–1976, <https://kns.cnki.net/kcms/detail/42.1874.p.20220623.1744.002.html>.
- [28] J. Wang, W. Jin, Y. Cui, W. Zhang, C. Wu, P. Alessandro, Earthquake-triggered landslides affecting a UNESCO natural site: the 2017 Jiuzhaigou earthquake in the World National Park, China, *J. Mt. Sci.* 15 (2018) 1412–1428, <https://doi.org/10.1007/s11629-018-4823-7>.
- [29] S. Ling, C. Sun, X. Li, Y. Ren, J. Xu, T. Huang, Characterizing the distribution pattern and geologic and geomorphic controls on earthquake-triggered landslide occurrence during the 2017 Ms7.0 Jiuzhaigou earthquake, Sichuan, China, *Landslides* 18 (2021) 1275–1291, <https://doi.org/10.1007/s10346-020-01549-6>.
- [30] M. Chang, P. Cui, L. Xu, Y. Zhou, The spatial distribution characteristics of coseismic landslides triggered by the Ms7.0 Lushan earthquake and Ms7.0 Jiuzhaigou earthquake in Southwest China, *Environ. Sci. Pollut. Res.* 28 (2021) 20549–20569, <https://doi.org/10.1007/s11356-020-11826-5>.
- [31] X. Guo, B. Fu, J. Du, P. Shi, J. Li, Z. Li, J. Du, Q. Chen, H. Fu, Monitoring and assessment for the susceptibility of landslide changes after the 2017 Ms7.0 Jiuzhaigou earthquake using the remote sensing technology, *Front. Earth Sci.* 9 (2021) 633117, <https://doi.org/10.3389/feart.2021.633117>.
- [32] L. Luo, X. Pei, C. Zhong, Q. Yang, X. Fan, L. Zhu, R. Huang, Multi-temporal landslide inventory-based statistical susceptibility modeling associated with the 2017 Mw6.5 Jiuzhaigou earthquake, Sichuan, China, *Front. Environ. Sci.* 10 (2022), <https://doi.org/10.3389/fenvs.2022.858635>, 200.
- [33] C. Xu, X. Xu, Statistical analysis of landslides caused by the Mw6.9 Yushu, China, earthquake of April 14, 2010, *Nat. Hazards* 72 (2014) 871–893, <https://doi.org/10.1007/s11069-014-1038-2>.
- [34] H.-B. Havenith, K. Guerrier, R. Schlögel, A.-S. Mreyen, S. Ulysse, A. Braun, K.-H. Victor, N. Saint-Fleur, L. Cauchie, D. Boisson, Earthquake-induced landslides in Haiti: seismotectonic and climatic influences, size-frequency relationships, *Nat. Hazards Earth Syst. Sci. Discuss.* (2022) 1–43, <https://doi.org/10.5194/nhess-2022-83>.
- [35] E.L. Harp, R.W. Jibson, R.G. Schmitt, Map of landslides triggered by the January 12, 2010, Haiti earthquake, *US Geol. Surv. Sci. Invest. Map* 3353 (2016) 15, <https://doi.org/10.3133/sim3353>.
- [36] C. Xu, X. Xu, Application and test of logistic regression model in risk assessment of Yushu earthquake landslide, *J. Eng. Geol.* 20 (2012) 326–333, <https://doi.org/10.3969/j.issn.1004-9665.2012.03.004>.
- [37] C. Xu, X. Xu, G. Yu, Landslides triggered by slipping-fault-generated earthquake on a plateau: an example of the 14 April 2010, Ms7.1, Yushu, China earthquake, *Landslides* 10 (2013) 421–431, <https://doi.org/10.1007/s10346-012-0340-x>.
- [38] W. Wu, The susceptibility analysis of landslides triggered by the 2014 Ludian earthquake, *Institute of Earthquake Forecasting, CEA*, 2018.
- [39] R. Liu, X. Yang, C. Xu, L. Wei, X. Zeng, Comparative study of convolutional neural network and conventional machine learning methods for landslide susceptibility mapping, *Rem. Sens.* 14 (2022) 321, <https://doi.org/10.3390/rs14020321>.
- [40] S. Ma, C. Xu, Y. Tian, X. Xu, Landslide hazard assessment of Jiuzhaigou earthquake based on logistic regression model, *Seismol. Geol.* 41 (2019) 162–177, <https://doi.org/10.3969/j.issn.0253.4967.2019.01.011>.
- [41] Z. Yang, C. Xu, X. Shao, S. Ma, L. Li, Landslide susceptibility mapping based on CNN-3D algorithm with attention module embedded, *Bull. Eng. Geol. Environ.* 81 (2022) 412, <https://doi.org/10.1007/s10064-022-02889-4>.
- [42] X. Chen, X. Shan, M. Wang, C. Liu, N. Han, Applying the newmark model in the assessment of earthquake triggered landslides during the 2017 Ms7.0 Jiuzhaigou earthquake, China, understanding and reducing landslide disaster risk: Volume 2 from Mapping to Hazard and Risk Zonation 5th, 2021, pp. 275–281, https://doi.org/10.1007/978-3-030-60227-7_30.
- [43] C. Xu, X. Xu, X. Wu, F. Dai, X. Yao, Q. Yao, Detailed cataloging of landslides in the 2008 Wenchuan earthquake and analysis of their spatial distribution, *J. Eng. Geol.* 21 (2013) 25–44, <https://doi.org/10.3969/j.issn.1004-9665.2013.01.004>.
- [44] F. Dai, C. Xu, X. Yao, L. Xu, X. Tu, Q. Gong, Spatial distribution of landslides triggered by the 2008 Ms8.0 Wenchuan earthquake, China, *J. Asian Earth Sci.* 40 (2011) 883–895, <https://doi.org/10.1016/j.jseae.2010.04.010>.
- [45] H. Yagi, G. Sato, D. Higaki, M. Yamamoto, T. Yamasaki, Distribution and characteristics of landslides induced by the Iwate–Miyagi Nairiku earthquake in 2008 in Tohoku District, Northeast Japan, *Landslides* 6 (2009) 335–344, <https://doi.org/10.1007/s10346-009-0182-3>.
- [46] C. Xu, J. Shyu, X. Xu, Landslides triggered by the 12 January 2010 Port-au-Prince, Haiti, Mw=7.0 earthquake: visual interpretation, inventory compiling, and spatial distribution statistical analysis, *Nat. Hazards Earth Syst. Sci.* 14 (2014) 1789–1818, <https://doi.org/10.5194/nhess-14-1789-2014>.
- [47] T.R. Martha, K.B. Govindharaj, K.V. Kumar, Damage and geological assessment of the 18 September 2011 Mw6.9 earthquake in Sikkim, India using Very high resolution satellite data, *Geosci. Front.* 6 (2015) 793–805, <https://doi.org/10.1016/j.gsf.2013.12.011>.
- [48] C. Xu, X. Xu, J.B.H. Shyu, Database and spatial distribution of landslides triggered by the Lushan, China Mw6.6 earthquake of 20 April 2013, *Geomorphol* 248 (2015) 77–92, <https://doi.org/10.1016/j.geomorph.2015.07.002>.
- [49] Y. Tian, C. Xu, X. Xu, J. Chen, Detailed inventory mapping and spatial analyses to landslides induced by the 2013 Ms6.6 Minxian earthquake of China, *J. Earth Sci.* 27 (2016) 1016–1026, <https://doi.org/10.1007/s12583-016-0905-z>.
- [50] C. Xu, S. Ma, Z. Tan, C. Xie, S. Toda, X. Huang, Landslides triggered by the 2016 Mj7.3 Kumamoto, Japan, earthquake, *Landslides* 15 (2018) 551–564, <https://doi.org/10.1007/s10346-017-0929-1>.
- [51] W. Wu, C. Xu, X. Wang, Y. Tian, F. Deng, Landslides triggered by the 3 August 2014 Ludian (China) M w 6.2 earthquake: an updated inventory and analysis of their spatial distribution, *J. Earth Sci.* 31 (2020) 853–866, <https://doi.org/10.1007/s12583-020-1297-7>.

- [52] X. He, C. Xu, W. Qi, Y. Huang, Y. Chen, B. Wen, A database of landslides triggered by 2014 Mw6.1 Jinggu earthquake, China, IOP Conference Series: Earth and Environmental Science, IOP Publishing, 2021 052008, <https://doi.org/10.1088/1755-1315/861/5/052008>.
- [53] C. Xu, Y. Tian, L. Shen, S. Ma, X. Xu, B. Zhou, X. Huang, J. Ma, X. Chen, 2015 Nepal Gurkha Mw7.8 earthquake landslide database, Seismol. Geol. 40 (2018) 1115–1128, <https://doi.org/10.3969/j.issn.0253-4967.2018.05.011>.
- [54] K.R. Gnyawali, B.R. Adhikari, Spatial relations of earthquake induced landslides triggered by 2015 Gorkha earthquake Mw=7.8, advancing culture of Living with landslides: Volume 4 Diversity of Landslide Forms, Springer, 2017, pp. 85–93, https://doi.org/10.1007/978-3-319-53485-5_10.
- [55] Y. Huang, C. Xu, X. Zhang, C. Xue, S. Wang, An updated database and spatial distribution of landslides triggered by the Milin, Tibet Mw6. 4 earthquake of 18 November 2017, J. Earth Sci. 32 (2021) 1069–1078, <https://doi.org/10.1007/s12583-021-1433-z>.
- [56] H. Tanyaş, K. Hill, L. Mahoney, I. Fadel, L. Lombardo, The World's second-largest, recorded landslide event: lessons learnt from the landslides triggered during and after the 2018 Mw7.5 Papua New Guinea earthquake, Eng. Geol. 297 (2022) 106504, <https://doi.org/10.1016/j.enggeo.2021.106504>.
- [57] Y. Cui, P. Bao, C. Xu, S. Ma, J. Zheng, G. Fu, Landslides triggered by the 6 September 2018 Mw6.6 Hokkaido, Japan: an updated inventory and retrospective hazard assessment, Earth Sci. Inf. 14 (2021) 247–258, <https://doi.org/10.1007/s12145-020-00544-8>.
- [58] X. Shao, S. Ma, C. Xu, P. Zhang, B. Wen, Y. Tian, Q. Zhou, Y. Cui, Planet image-based inventorying and machine learning-based susceptibility mapping for the landslides triggered by the 2018 Mw6. 6 Tomakomai, Japan earthquake, Rem. Sens. 11 (2019) 978, <https://doi.org/10.3390/rs11080978>.
- [59] X. Shao, S. Ma, C. Xu, Distribution and characteristics of shallow landslides triggered by the 2018 Mw7.5 Palu earthquake, Indonesia, Landslides 20 (2023) 157–175, <https://doi.org/10.1007/s10346-022-01972-x>.
- [60] Y. Huang, C. Xu, X. Zhang, Spatial distribution and influence factors of landslides triggered by the 2019 Ms6.0 Changning, Sichuan, China Ms6. 0 earthquake: a statistical Analysis based on QGIS, IOP Conference Series: Earth and Environmental Science, IOP Publishing, 2021 052007, <https://doi.org/10.1088/1755-1315/861/5/052007>.
- [61] X. He, C. Xu, Spatial distribution and tectonic significance of the landslides triggered by the 2021 Ms6. 4 Yangbi earthquake, Yunnan, China, Front. Earth Sci. 10 (2022) 1030417, <https://doi.org/10.3389/feart.2022.1030417>.
- [62] B. Zhao, Y. Wang, W. Li, H. Lu, Z. Li, Evaluation of factors controlling the spatial and size distributions of landslides, 2021 Nippes earthquake, Haiti, Geomorphol 415 (2022) 108419, <https://doi.org/10.1016/j.geomorph.2022.108419>.
- [63] Z. Xiao, C. Xu, Y. Huang, X. He, X. Shao, Z. Chen, C. Xie, T. Li, X. Xu, Analysis of spatial distribution of landslides triggered by the Ms6.8 Luding earthquake in China on September 5, 2022, Geoenviron, Disasters 10 (2023) 1–15, <https://doi.org/10.1186/s40677-023-00233-w>.